H3.4

Non-destructive evaluation[†]

Hans-Joachim Krause, Michael Mück and Saburo Tanaka

H3.4.1 Introduction

With the development of complex machinery and structures designed for long-term usage, the need for inspecting them became apparent in order to avoid failures. The most common inspection techniques include visual inspection, radiography, ultrasonics, acoustic emission, and electromagnetic techniques such as eddy current testing (Bray and Stanley 1989). These methods are subsumed under the terms "non-destructive evaluation" (NDE) or "non-destructive testing" (NDT). The development of NDE techniques has essentially been very problem-specific. There is no universal technique which can be applied to the majority of NDE problems. Electromagnetic techniques such as eddy current testing probe the electromagnetic properties of the sample under test. Faraday coils (also called induction coils or pickup coils) are the most popular sensors for this methodology because of their simplicity and versatility. However, Hall probes, fluxgates and magnetoresistors are also used as magnetic field detectors. SQUID sensors are the most sensitive sensors for magnetic flux and field known to date, particularly at low frequencies. SQUIDs have been used for NDE since the 1980s. SQUID-based electromagnetic NDE techniques are particularly well suited for inspection of thick metallic structures because the required penetration

[†] This chapter is dedicated to the memory of Gordon B. Donaldson (1941 – 2012) who wrote the NDE chapter for the first edition of this book.

depth can be achieved with low frequency magnetic fields. Both low- and high-T_c SQUIDs have been used as sensors for magnetic detection of both surface breaking and deep lying flaws in different metals including iron, steel, aluminium and titanium.

The chapter is organized as follows. At first, a brief overview of the challenging NDE requirements demanding SQUID usage is given (chapter H3.4.2). Then, the basic principles of electromagnetic NDE using SQUIDs in static and in alternating magnetic fields are explained. A concise review of prior work is given. Selected examples are described in more detail. The methods employed are magnetic flux leakage (chapter H3.4.3), in which the defect is polarized by a magnetic field, and the induced dipole or higher order magnetic moment is detected by a SQUID. A special case is the detection of magnetic inclusions in non-magnetic base material which are magnetized by passing the specimen through a strong magnetic field before measurement (chapter H3.4.4). A very common technique is eddy current testing in which an incident AC magnetic field induces eddy currents in the electrically conducting specimen, possible flaws distort the flow of eddy currents, and the SQUID measures the subsequent distortion of the magnetic field generated by these currents (chapter H3.4.5). The spatial resolution of these techniques is significantly enhanced if the stand-off between flaw and sensor is reduced, as achieved in so-called SQUID microscopes (chapter H3.4.6). These methods have been applied for non-destructive evaluation (NDE) before SQUID sensors became available. The reasons for replacing conventional magnetic field sensors with SQUIDs, in spite of their need for cooling, are (a) unsurpassed magnetic field sensitivity, (b) large dynamic range which allow to measure minute field changes in the presence of large exciting fields, and (c) frequency-independent sensitivity, allowing usage of lower frequencies and thus detection of faults at greater depths than in conventional eddy current measurements.

H3.4.2 History and challenges

The use of SQUIDs in NDE was pioneered by Gordon Donaldson’s group at the University of Strathclyde and by Harold Weinstock at the U.S. Air Force Office of Scientific Research. A challenge for the petroleum industry is to find cracks and corrosion in submerged pipelines, often coated with plastic or concrete and possibly marine growth. Ultrasonic methods will find the flaws, but require complete removal of the coating and cleaning, which is very expensive in operator costs. Among the first experiments were the remote detection of surface breaking cracks in ferromagnetic steel (Bain *et al.*, 1985), a study of plastic deformation in magnetic steels (Evanson *et al.*, 1989) and the localization of metal pipelines (Weinstock and Nisenoff, 1985).

Similarly, work hardening of steel due to flexure can be detected, because in the work hardened region, the permeability reduces from about 800 to about 400. Donaldson *et al.* (1990) showed that heat damage in ferritic stainless steels can be detected by first saturating the ferritic phase in an applied field and subsequently detecting its remanence with a SQUID. Prolonged heat treatment of the steel results in progressive magnetic hardening, with the result that the saturation magnetization changes little, but the remanence increases, so that taking the ratio of the two signals at a given point is a measure of the local heat damage.

Another very challenging NDE application is the inspection of reactor vessels and similar structures in chemical and nuclear plants. Many such plants are to be used for periods considerably longer than their design lives, and it is necessary to detect any weakening of structures due to strain and corrosion, and heat and radiation damage. The field gradient distribution of hardened steel cylinders was studied with a HTS SQUID to detect mechanical stress in such cylinders (Wunderlich *et al.*, 1998). An alternate approach to evaluate hysteresis effects of iron samples is

to measure its Barkhausen noise (Weinstock *et al.*, 1985). The magnetic response to stress-strain hysteresis cycles in steel has been studied with SQUID (Banchet *et al.*, 1995).

A closely related NDE challenge is the detection of corrosion. The direct approach aims at the detection of the electrical corrosion currents characteristic for ongoing active corrosion. Electrolytic corrosion processes were studied in non-voltaic cells (Bellingham *et al.*, 1987). Corrosion currents were measured with a SQUID array (Hibbs *et al.*, 1993). The indirect posterior approach is to measure the results of corrosion, i.e. the reduction of cross-section and the appearance of cracks in steel reinforcing bars. Tendon cracks in the concrete structure of a highway bridge were measured with a portable HTS SQUID (Krause *et al.*, 2002).

The detection of deep lying cracks and corrosion is an important issue particularly for ageing aircraft as they can produce structural failures. The most dramatic demonstration of this was the 1988 partial loss of the outside skin of an airborne Aloha Airlines B737, caused by deep lying corrosion and cracking at riveted joints in the airframe. For flaws lying at depths of more than 10 mm in aluminium structures, conventional eddy current testing comes to its limits because induction coils become too insensitive at the required frequencies below 1 kHz. Eddy-current-testing experiments were carried out at the National Bureau of Standards (Capobianco *et al.*, 1986). Nondestructive testing of aircraft parts using eddy current techniques has been widely explored, for example, by (Wikswo, 1995; Hohmann *et al.*, 1999; Kreutzbruck *et al.*, 1999; Ruosi *et al.*, 1999),

Further work can be found in reviews of SQUID NDE (Kreutzbruck, 2004; Clarke and Braginski, 2006; Krause and Donaldson, 2006; Krause *et al.*, 2015).

H3.4.3 Magnetic flux leakage

Magnetic flux leakage terms a measurement technique where static magnetic fields are used to enhance changes in the magnetic field produced by defects in the material under test. The basic testing configuration is outlined in Fig. 1. The sample is magnetized in a static magnetic field B applied by a permanent magnet. A sample with a uniform magnetic susceptibility χ will just produce magnetic fields at its edges. If the sample contains a local inhomogeneity, i.e. an inclusion of volume V and susceptibility $\chi + \delta\chi$, then the field will generate a magnetic dipole $m = \delta\chi VB$. When the sample is scanned relatively to a magnetometer, i.e. a SQUID, the inclusion will generate a distortion field $\Delta B \sim \chi VB_{loc}/h^3$ that can be measured by the magnetometer at a distance h from the flaw. The information thus gained by this experiment is about a variation in the susceptibility of the sample. Provided ΔB is above the threshold limit for the magnetometer, then this becomes a means for detecting the inclusion.

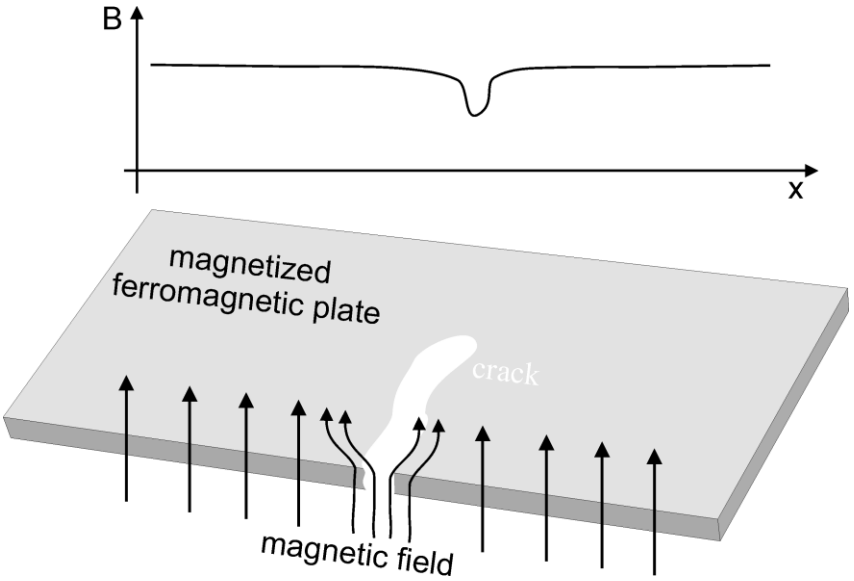

Fig. 1. Basic principle of nondestructive evaluation of ferromagnetic plates using a magnetic field sensor, such as a SQUID (see text).

In principle, any magnetic sensing device could be used for detecting ΔB. The key feature of the SQUID based magnetometer is that even if the polarizing field is of the order of 1–50 mT, the SQUID magnetometer will retain its full sensitivity to changes ΔB, which could ideally be as little as 1 fT $Hz^{-1/2}$. This is due to the SQUID’s flux-to-voltage characteristics which is periodic in the magnetic flux quantum Φ_0. In practice, even sensitivities of 50 fT $Hz^{-1/2}$ in case of low-T_c SQUIDs or 300 fT $Hz^{-1/2}$ for high-T_c represent an extremely large dynamic range which is 3 to 4 orders of magnitude better than that of conventional magnetic sensors. This improvement has been the key to the larger standoffs and the detection of smaller flaws, which have been realized with magnetometric SQUID NDE. As static fields have to be detected, and environmental magnetic noise has a large 1/f component, the testing has usually to be done in a magnetically shielded environment. If the samples under test are small, a small mu-metal box will be sufficient to suppress environmental noise.

At the University of Strathclyde, flaws were in ferric steel plates with this approach (Bain *et al.*, 1985; Evanson *et al.*, 1989; Evanson *et al.* 1993; Donaldson *et al.*, 1996). They were able to find small slots in such plates with distances between the slot and the SQUID of up to 10 cm. The laws of magnetostatics yield that the spatial resolution of a magnetic flux leakage measurement will be the larger of the pick-up coil diameter and the stand-off distance. At typical stand-off distances of several cm, localization of a flaw will be much less precise than flaw size, which is typically ~ mm. However, the intended application was to provide a rough location of corrosion flaws underneath the surface coatings, such as marine growth and concrete, on undersea oil-pipes, to eliminate the need for cleaning the entire pipe before the detailed ultrasonic or other inspection which would locate the flaw precisely. The issue of achieving high spatial resolution with the SQUID method therefore did not arise. However, the method turned out to be of little use in

detecting flaws at welds, the sites of most common appearance. It proved impossible to distinguish flaws from the welds themselves because heat treated steel is itself a source of large permeability variation.

Magnetic detection is well suited to evaluate phase changes in magnetic materials, like the emergence of a magnetic martensitic phase in austenitic base material. Mechanical fatigue in structural steel was detected with a SQUID (Bonavolontà *et al.*, 2009). The so-called white layer on rails, a martensitic texture generated by the rapid heating and cooling due to spinning train wheels, were detected with a high-T_c SQUID (Miyazaki *et al.*, 2012). The technique is not limited to metals. Flaws and voids representing local inhomogeneities of the magnetic susceptibility were detected even in nonmagnetic plexiglass (Thomas *et al.*, 1993) by measuring the magnetic leakage flux.

Magnetic flux leakage using static magnetic fields was also applied for the inspection of prestressed steel tendons in concrete beams or bridge decks (Sawade *et al.*, 1997; Ghorbanpoor, 1998; Sawade and Krause, 2010). Tendon ruptures may occur when water penetrates the duct due to inadequate grouting. Hydrogen-induced corrosion of the steel tendons may then be initiated, which will eventually cause cracks of single strands and could finally lead to a collapse of the entire structure. The basic principle of magnetic flux leakage is as follows. Tendons hidden in the concrete are magnetized by a static magnetic field applied from outside the concrete by means of a yoke magnet. The tendon can be considered as a high-permeability magnetic field guide. Ruptures or reductions of its cross-section produce a resulting magnetic leakage flux as they act as local disturbances in the flux guide. The ensuing magnetic stray field is then recorded. To this end, a probe containing the magnetization device (yoke magnet) and the magnetic field sensors is moved along the direction of the prestressed tendon on the concrete surface (see Fig. 2).

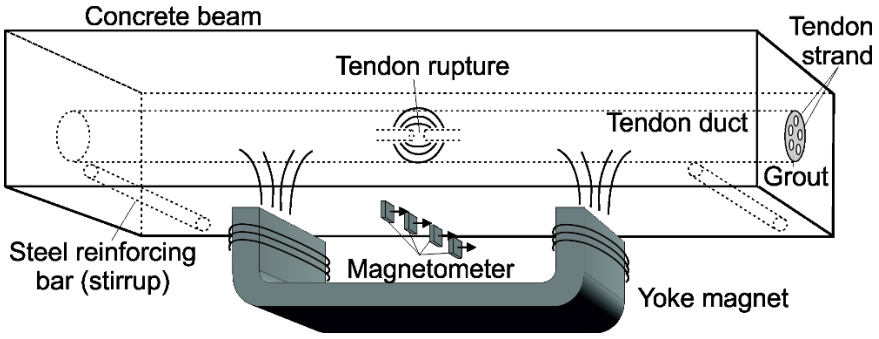

Fig. 2. Principle of magnetic detection of ruptures in tendon strands of prestressed concrete beams.

This technique was employed to evaluate tendons inside highway bridges (Krause *et al.*, 2002; Sawade *et al.*, 1997). Four high-T_c dc SQUID magnetometers with ramp junctions optimized for high-field performance (Faley *et al.*, 1999) were used to detect the magnetic stray field in the center of the yoke. The magnetic field was recorded while the exciting field was applied (active stray field measurement) and again after the magnet had been switched off (remanent field measurement). It was shown that a single cracked rebar can be found in post-tensioned members, even though the magnetic signature of the crack is attenuated significantly by the shielding effect of the surrounding flawless tendons and the duct around the strands. Before each measurement scan, the SQUID sensors were heated just above the critical temperature of the superconducting film in order to eliminate trapped magnetic flux. Details on the signal analysis procedure were published in (Sawade and Krause, 2010a). Correlation analysis of the measured stray field and remanent field scans with sample crack signals yielded the locations and the approximate size of submerged cracks. Opening the bridge deck confirmed the presence of the cracks at the indicated locations.

H3.4.4 Detection of magnetic inclusions

Aircraft turbine rotor problems emerged as rotation speeds increased in new generations of engines. Ferrous impurity inclusions in the titanium base alloy can weaken the strength of the blade root disc, leading to failure under the centrifugal forces exerted by the attached blades. A major US air accident was found to be due to such impurities, which are not x-ray detectable. A high-T_c SQUID-based test was in routine use for BMW-Rolls-Royce in the late 1990’s (Tavrin *et al.*, 1999). The turbine disks were subjected to a magnetic field, which polarizes any such inclusions. The resultant fields were then detected using a high T_c SQUID with a sensitivity of about 130 fT/Hz$^{1/2}$. With a second order gradiometer, a ferritic mass of 1 mg was detected at a depth of 70 mm while 10 µg was seen at a depth of 4 mm.

NbTi/Cu wires were tested for defects by passing them underneath an HTS dc SQUID (Weinstock *et al.*, 1999). A similar technique was applied to the detection of ferromagnetic inclusions in various industrial products (Krause *et al.*, 2005; Bick *et al.*, 2005; Tanaka *et al.*, 2006). Saburo Tanaka’s group at Toyohashi University of Technology developed a system which is used to detect magnetic contaminants in (canned) food products (Tanaka *et al.*, 2006; Tanaka *et al.*, 2007; Nagaishi *et al.*, 2007) and active-material coated foils for Li-ion batteries (Tanaka *et al.*, 2009). Examples of these contaminants in both, metallic foils as well as food, are small metal chips from raw materials or the processing machinery. The current requirements for commercial applications, such as Li-ion batteries, are to find metallic particles that have a diameter greater than 50 µm. However, particles smaller than about 100 µm cannot be detected by X-ray imaging, which is commonly used as the inspection method. For this reason, Tanaka *et al.* (2006) developed a highly sensitive detection system for small contaminant particles based on a high-temperature-

superconductor (HTS) SQUID. They use a planar gradiometer and a horizontal magnetization of the sample prior to measurement.

The principle of detecting magnetic contaminants with their system is shown in Fig. 3. A permanent magnet with a flux density of 1.3 T horizontally magnetizes the metallic contaminants and the test object itself. The remanent magnetic flux from a possible metallic contaminant in the sheet is then detected by a number of SQUID gradiometers (4 x 2 Array) as the sheet passes below these sensors. The inset shows the picture of the SQUID array through a vacuum window. Sheets with a maximum width of 100 mm can be tested with a maximum speed of 100 m/min. The detection unit including the shield and the cryostat is mechanically well isolated from the magnet and the driving components, in order to protect them from mechanical vibrations. The dimensions (length × width × height) of the entire system are 2200 mm × 700 mm × 1380 mm. For food contaminant detection, the requirement for the detection size is greater than 0.5 mm in diameter. A major Japanese dairy company introduced and equipped a high Tc SQUIDs detection system in 2005; this system is still in use every day in the factory (Nagaishi *et al.*, 2007; Braginski, 2011).

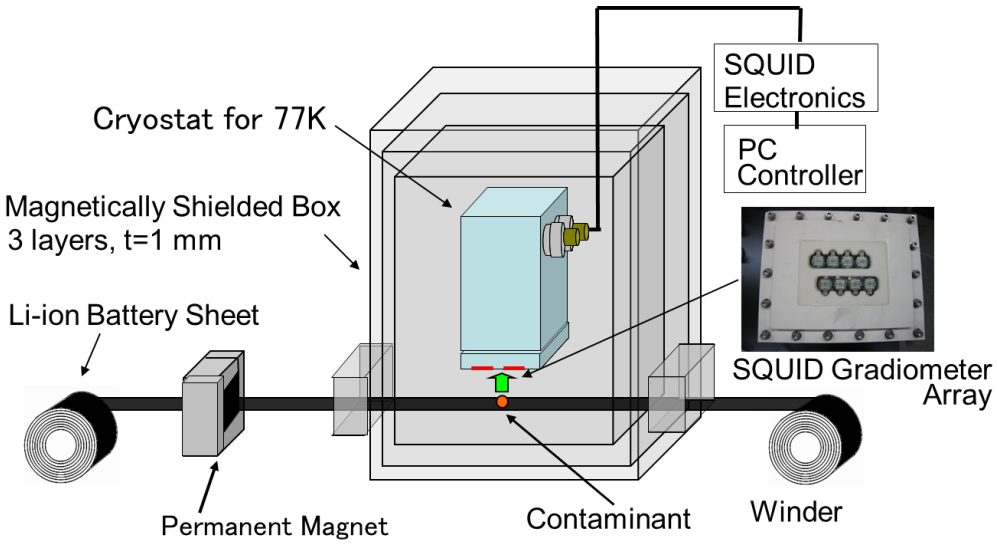

Fig. 3. Principle for detection of contaminants in metallic sheets.

The liquid nitrogen (LN_2) cryostat used for maintaining the temperature of the eight SQUID gradiometers at 77 K is custom designed. The outer jacket of the cryostat is fabricated from aluminum alloy, and the LN_2 tank is made from copper. The total volume of LN_2 is 1.1 ℓ, which is sufficient for 14-h operation without refilling. In order to achieve a small standoff-distance between the SQUIDs and the sample under test, the SQUIDs are placed inside the insulation vacuum of the dewar, rather than immersed in the LN_2. To thermally anchor the SQUIDs to the LN_2 bath, they are mounted to eight sapphire rods protruding through the bottom of the LN_2 container into the insulation vacuum. In this configuration, the sample under test can be placed as close as 1–2 mm to the SQUIDs (Tanaka *et al.*, 2011). The dewar containing the SQUIDs is placed inside a small magnetic shield to suppress external magnetic fields. This shield measures 630 mm × 480 mm × 704 mm, and is made from 2-mm thick mu-metal. The measured shielding factors (*SF*) of the magnetically shielded box for each direction at 1 Hz are SF_x = 50,000, SF_y = 33,000, and SF_z = 25,000. These factors are sufficient for operation in a typical laboratory or industrial environment.

The white noise level of the SQUID gradiometers employed is 20–30 $\mu\phi_0/\mathrm{Hz}^{1/2}$ at 100 Hz. These values are 10 $\mu\phi_0/\mathrm{Hz}^{1/2}$ higher than the values measured when the SQUIDs are immersed in LN_2 because of the relatively high temperature of the sapphire rods (T > 77 K). The base-line lengths of the gradiometers are 3 mm. Three SQUID loops are directly connected to a differential pickup loop consisting of rectangular pickup loops (3 mm × 8 mm for each loop). For data post-processing, the signal is passed through a high-pass filter with a cutoff frequency of 0.5 Hz, and a second-order low-pass filter with a cutoff frequency of 100 Hz.

Small iron (S50C) balls with a diameter of 35–82 μm are used to characterize the system. The balls are first magnetized by the permanent magnet, and their remanent field is measured with

the SQUID gradiometers. Real-time traces of the gradiometer output at sheet speeds of 9 m/min and 50 m/min are shown in Fig. 4. Even the smallest balls at higher speed 50 m/min produce a typical gradiometric signature with a high signal-to-noise ratio.

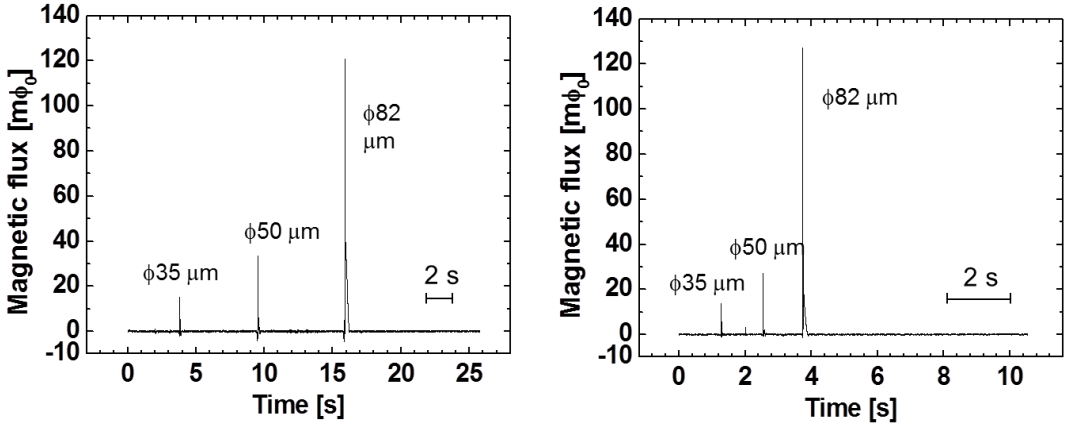

Fig. 4. Left: Signal time trace of small metallic ball with different diameter at sheet speed of 9 m/min, and right: Signal time trace of small metallic ball with different diameter at sheet speed of 50 m/min.

Tsukada *et al.* performed high-Tc SQUID-based measurements of the magnetic susceptibility of soil, concrete, and glutinous rice. They determined the moisture of these samples by measuring their reduced magnetization with increased water content due to the diamagnetic properties of water (Tsukada *et al.*, 2017). In case of the rice samples, a rotating sample technique was used to pass the sample through a strong magnetic field of 500 mT and measure its stray magnetic field. The soil samples were measured by recording their nonlinear magnetic susceptibility in a 10 mT, 10 Hz alternating magnetic field with 400 mT static bias field.

Hatsukade *et al.* reported a novel SQUID-NDE technique for pipes combining SQUID and ultrasonic guided waves (Hatsukade *et al.*, 2017). Measurements of magnetic signals due to acoustic emission and ultrasonic guided waves were demonstrated. To convert the guided waves into magnetic signals, the inverse magnetostrictive effect of a magnetized nickel thin plate glued around the pipe’s circumference was utilized.

H3.4.5 Eddy current testing

Eddy current testing is a well-established procedure to test electrically-conducting objects for defects. With an AC magnetic field, eddy currents are induced in the sample under test. If the object has homogeneous conductivity, i.e., no defects are present, the local eddy current density will be homogeneous as well. Defects will locally change the conductivity and thus lead to a distortion of the eddy current flow in the vicinity of the defect (see Fig. 5, left).

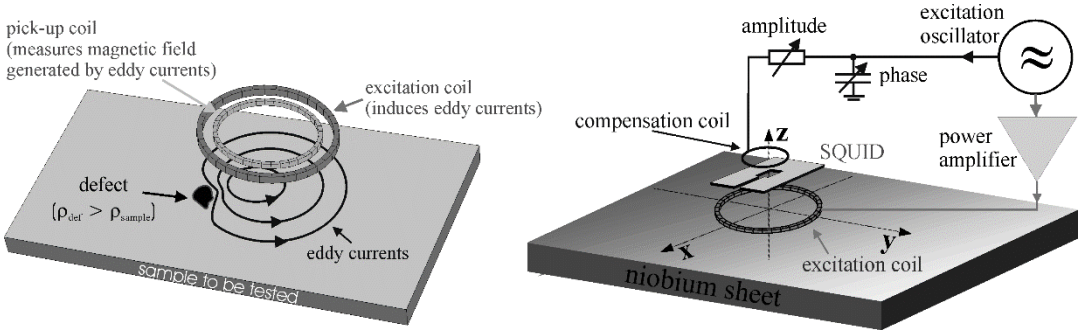

Fig. 5. Basic principle of eddy current NDE (left), and measurement configuration used to test niobium sheets with a SQUID (right).

A conventional eddy current NDE system consists of an excitation coil system, which creates currents in the test object. Defects can obviously be localized by measuring the local eddy current density. As a direct measurement of the eddy currents is difficult, one rather measures the magnetic field produced by the eddy currents directly above the sample. In a conventional eddy current test set, the magnetic field produced by the eddy currents (sometimes called the secondary field to distinguish it from the primary field, which is used to induce the eddy currents) is measured with a pickup coil (shown in Fig. 5 left). Anomalies in the magnetic field of the eddy current are caused by spatial diversion of the eddy currents when they encounter flaws such as corrosion and cracks. According to Faraday’s law of induction, the coil detects the time derivative $d\phi/dt$ of the flux threading the coil. Thus, the induced signal is proportional to excitation frequency f. Thus, the sensitivity for finding defects scales as $1/f$. However, low frequencies are required to detect deep

lying flaws because the eddy currents extend only to approximately two or three times the skin depth, given by $\delta = (\pi\sigma f \mu_0\mu_r)^{-1/2}$, where f is the frequency, σ the electrical conductivity, μ_r the relative permeability of the material, and $\mu_0 = 4\pi\times10^{-7}$ H/m the magnetic permeability of vacuum. At 1 kHz, δ is 3.4 mm in aircraft aluminium ($\sigma = 2.2\times10^7\ \Omega^{-1}\text{m}^{-1}$). This sets the approximate upper limit to flaw detection depth with conventional eddy current instrumentation, because eddy currents decay exponentially with increasing depth, and it is hard to detect frequencies below 1 kHz with Faraday coils. In materials with lower electrical conductivity such as indium-tin oxide (ITO, $\sigma \approx 1\times10^5\ \Omega^{-1}\text{m}^{-1}$), much larger penetration depths are achieved. That means that much higher frequencies can be used.

In contrast to Faraday induction coils, SQUIDs retain their sensitivity down to zero frequency because they measure changes in the magnetic flux ϕ, rather than $\text{d}\phi/\text{d}t$. This means that they can detect flaws at very large depths. To reach to a skin depth of δ = 34 mm into an aircraft structure, it would be necessary to operate at f = 10 Hz, which is probably the lowest practicable frequency if one is going to scan a structure at a reasonable rate (say 2 mm/s). The high field sensitivity of SQUIDs at low frequencies makes it ideally suited for the evaluation of such relatively thick conductive objects.

There are several ways to induce electric currents in the sample to be tested. A dc or ac current can simply be induced by connecting the sample with two wires to a power supply (Wikswo, 1996). This so-called direct current injection has several disadvantages: wires have to be attached to the sample, which —depending on the shape of the sample— might be difficult. It might also be difficult to determine the actual current distribution, and the obtainable current density might be low in case of a large-area sample. The signals, which potential defects might produce, will be only small for low current densities.

In contrast to direct injection of dc or ac currents into the sample, the induction of eddy currents by an external coil (usually called excitation coil) generates a spatially well-confined current distribution. As no electrical connections to the sample are required, eddy current NDE is more practical to use than direct current injection. Also, by choosing an appropriate coil geometry, the current density at potential defects can be made much higher. However, the choice of the optimum measurement parameters, such as the excitation frequency, is more critical. Furthermore, calculation of the current distribution in the sample from the measured field distribution tends to be more difficult than in the case of direct current injection. As usually users of NDE systems are not much interested in the current flow in the sample, but rather want to find defects, this is not a big disadvantage.

In order to minimize the excitation field at the location of the SQUID, a gradiometric excitation coil, a so-called double-D coil can be used (Tavrin *et al.*, 1996; Hohmann *et al.*, 1999; Kreutzbruck *et al.*, 1999; Ruosi et al, 1999). By carefully moving this coil below the SQUID to find its optimum position, the cross talk between excitation coil and SQUID can be kept lower than 0.1%. Alternatively, the magnetic field of a circular excitation coil can be compensated electronically at the location of the SQUID by passing part of the excitation current in the modulation coil used for flux locking the SQUID. By carefully adjusting the amplitude and phase of the compensation current, the excitation field at the SQUID can be reduced by a factor of up to 1000. An even higher compensation factor is, in principle, possible, but drift then requires a frequent readjustment of amplitude and phase of the compensation current. As the obtainable signal-to-noise ratio is directly proportional to the amplitude of the excitation field, the latter should be as large as possible. Field amplitudes of mT should be aimed at.

A number of groups have studied eddy-current testing procedures with a low T_c SQUID (Wikswo, 1995) or with a high T_c SQUID (Hohmann *et al.*, 1999; Kreutzbruck *et al.*, 1999; Ruosi *et al.*, 1999). The main interest here was in testing aircraft parts. Besides conventionally used aluminum and titanium alloys, carbon-fibre reinforced plastics were investigated (Ruosi *et al.*, 2002; Graham *et al.*, 2004; Bonavolontà *et al.*, 2004; Bonavolontà *et al.*, 2007; Hatsukade *et al.*, 2013). Such polymers have become increasingly popular in aircrafts because of their high specific stiffness and high specific strength.

Phase analysis allows to determine the depth of a flaw or to do depth-selective analysis of eddy currents (Ma and Wikswo, 1995; Wikswo, 1996; Lima *et al.*, 2006). They used sheet inducer technology to achieve very homogeneous eddy current distributions. The technique can be used to suppress surface flaw and thus achieve a relative enhancement of deep-lying flaws. Phase analysis has also been shown applicable to double-D excitation (Horng *et al.*, 2002). They showed that phase of the spatial field derivative dB/dx at the location of the flaw, which can be determined from the in-phase and quadrature components, scales linearly with the flaw depth.

Especially for aircraft fuselage inspection, a mobile SQUID system is needed which can be moved along the curved structures. Mobile high-T_c SQUID systems suitable for that purpose have been shown (Krause *et al.*, 1997; Keenan and Romans, 2012; Yoshida *et al.*, 2014).

A continuing issue in the aircraft maintenance industry is the development of cracks in airplane wheels. The standard testing procedure is to do manual ultrasonic testing from the inside which requires laborious dismantling of heat shields. A system using a high-T_c SQUID magnetometer with Joule-Thomson cooling in conjunction with remote eddy current excitation was developed to perform automated wheel testing from the outside (Hohmann *et al.*, 2001). The system proved to operate well in the electromagnetically disturbed environment at Lufthansa Base,

Frankfurt/M., airport. The cold head with the SQUID is moved along the wheel contour by a robot while the wheel rotates, thus generating an eddy current map of the outer wheel surface. The key structure of the inside of the wheel produces its own signature which repeats with each rotation, but among that signature, any crack produces an additional peak (Fig. 6). Analysis of the response field of an inside crack as a function of excitation coil displacement, eddy current frequency, and lock-in phase angle yielded an optimum wheel rotation velocity for deep-lying defects. The technique provides depth selectivity: signals from deep flaws are enhanced over surface flaws. Tests were conducted on aircraft wheels with known flaws. On a Boeing 737 wheel, an inner flaw penetrating only 10% of the wall thickness was detected by scanning the outside surface of the rim. Even though performance was better than conventional methodology, the SQUID system was not commercialized due to cost issues.

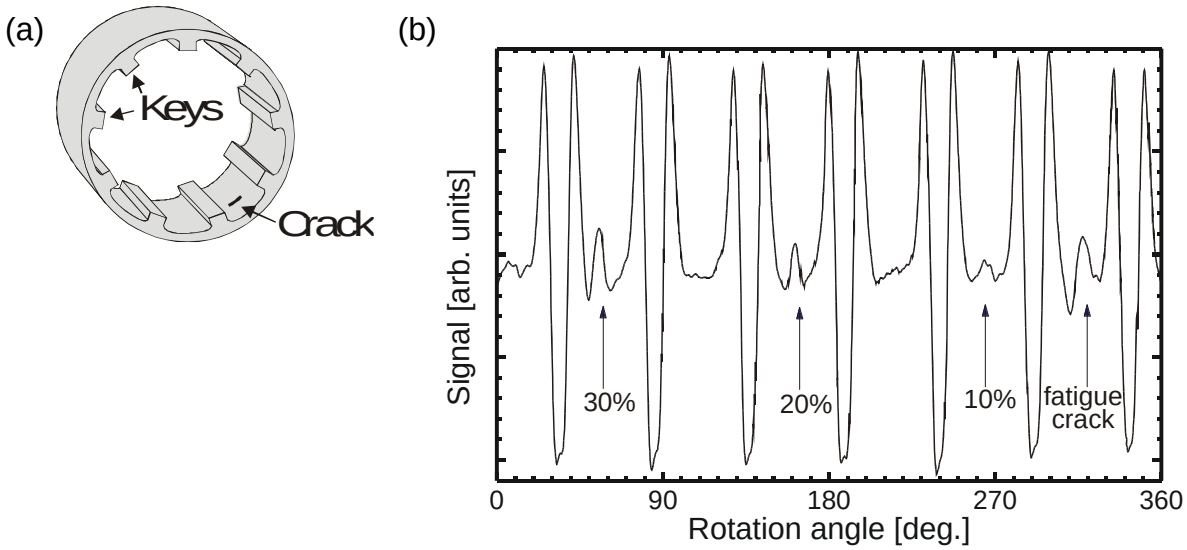

Fig. 6. In-phase SQUID signal track recorded in one rotation of Airbus wheel with artificial inner flaws.

A LTS SQUID-based eddy-current NDE system was studied to test flat niobium sheets used to make superconducting resonators for particle accelerators (Welzel, 2003; Mück *et al.*, 2003).

Such niobium sheets (usually of size 300 × 300 mm^2) have to be tested for small inclusions of foreign materials, such as tantalum, as these deteriorate the quality factor of the superconducting resonator made from such sheets. The requirements here are the detection of tantalum inclusions having a volume of as small as 10^{-12} m^3 in a short time; the time needed to test a 30×30 cm^2 sheet should not be longer than a few minutes, to be able to test a large number of sheets in an acceptable time. We discuss this system in some detail, as it gives a good example of a highly-sensitive SQUID eddy-current NDE system.

Fig. 5 (right) shows the principle of eddy current testing of a niobium sheet. A circular coil, usually with a diameter of a few mm, generates eddy currents in the niobium sheet. Inhomogeneities, such as cracks or inclusions of materials having a conductivity different from that of niobium, lead to a distortion of the eddy current flow, and thus to a change in the eddy current field, which is detected by scanning the sheet with a niobium SQUID. As a high spatial resolution is usually required, a circular excitation coil with diameter ~ 2 mm was used instead of the usual double-D coil; the excitation field at the SQUID was reduced by electronic compensation. In this example, the excitation field was of up to 1 mT peak-to-peak; the required excitation current was about 2 A peak-to-peak. Dissipation in the excitation coil raised its temperature to about 60°C in this case. Finally, the SQUID was cooled in a low-noise fiberglass helium dewar for biomagnetic measurements, permitting a small stand-off distance between SQUID and sample of about 6 mm.

The optimum excitation frequency is given by the skin depth in the material under test and the expected depth of the inclusions. In a superconducting resonator, rf currents will only flow at the surface of the resonator, so in principle one would only need to find defects in a depth of a few μm. However, during fabrication of the resonator, up to 0.5 mm of niobium are etched away from the surface, so that even defects in this depth might lead to a reduction in the obtainable resonator

quality factor. In order to maximize the eddy-current density in a 0.5 mm thick layer at the surface of the sheet, an excitation frequency of about 40 kHz would be required. Although the excitation field at the location of the SQUID is minimized by the compensation coil, a dynamic range of about 20 to 50 flux quanta is still needed at this frequency to prevent unlocking of the flux-locked loop by scanning across the edges of the sheet. The slew rate required of the flux-locked loop then is about 4 to 10 $\Phi_0/\mu s$, which can easily obtained with a conventional ac flux-modulated flux-locked loop with a modulation frequency of 4 MHz; a dynamic range of about 15 flux quanta at 100 kHz is possible.

A niobium dc SQUID was used in a magnetometer configuration with a field-to-flux transfer coefficient of 35 nT/Φ_0 (Welzel, 2003; Mück *et al.*, 2003); its flux noise was about 1.5 $\mu\Phi_0/\sqrt{Hz}$, and the field sensitivity was about 50 $fT/\sqrt{Hz}$. Much higher field sensitivities are possible of course, but since the thermal noise of the (room temperature) sample limits the useful sensitivity, it is wiser to make the inductance of the SQUID relatively small to achieve a low flux noise. A low inductance in turn leads to a relatively small effective area of the SQUID, which increases the dynamic range and thus the slew rate of the system. Because of the high excitation frequency of > 10 kHz and using lock-in detection, the system could be operated unshielded. With this system, Mück *et al.* (2003) were able to detect all relevant defects in high-purity niobium sheets in an acceptable time with a high signal-to-noise ratio.

Fig. 7, left, shows a typical example of an eddy-current scan of such a sheet using a SQUID. A typical value for the change in the eddy current field induced by a 100-μm diameter Ta inclusion in a depth of 0.5 mm was about 30 pT. Although it seems possible to detect this field with a conventional magnetic field sensor, such as a flux gate, the then intolerably long measuring time would make the use of such a sensor impractical. For example, a flux gate with a rms field noise

of 10 pT/√Hz could detect a Ta inclusion with a signal-to-noise ratio SNR ≈ 1 in an integration time of 1 s. Assuming the area covered by the flux gate is 1 mm^2, it would take 300 × 300 s to scan a 30 × 30 cm^2 wide niobium sheet. Not only is this measuring time intolerably long, also an SNR ≈ 1 is insufficient to discriminate between noise and real defects. The desired SNR for relevant defects is > 30.

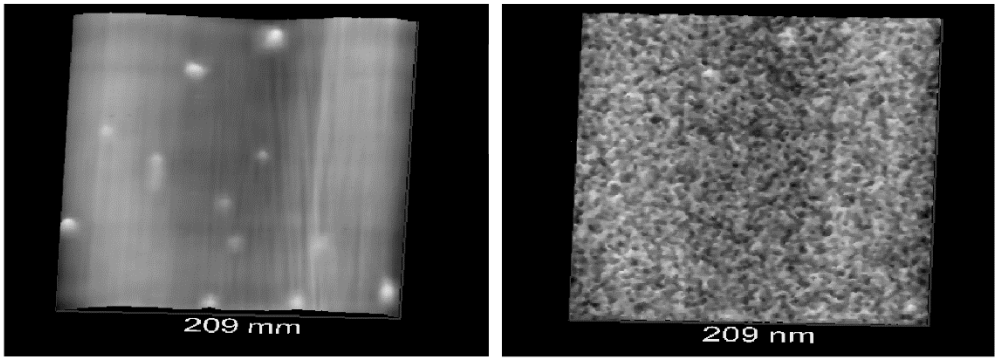

Fig. 7. Left: Two-dimensional distribution of the eddy current field above a 22 cm by 22 cm size niobium sheet. The excitation field generated by a 3-mm diameter coil was about 0.6 mT peak-to-peak; the eddy-current frequency was 10 kHz, measurement time was about 15 minutes. Ta inclusions (bright spots) are clearly detected. Right: Same sheet measured with conventional eddy-current NDE system. Most defects are obscured by noise. Scanning time and measurement bandwidth same as for SQUID measurement.

A drawback of eddy-current testing is the so-called 'lift-off effect'. Here, a variation in the stand-off distance between excitation coil and sample, for instance due to an uneven sample surface, leads to a change in the eddy current density in the sample, and thus to a change in the eddy current field detected by the SQUID. Already small variations in the stand-off distance of the order of 10 μm produce field changes larger than the response from a Ta inclusion in the example described above. Pressing the excitation coil firmly onto the sample during scanning can reduce the lift-off effect caused by roughness of the sample. Nevertheless, when scanning the surface of the sample using a high excitation frequency (100 kHz), the lift-off effect is still noticeable. Spatial

high-pass filtering can reduce artefacts caused by the lift-off effect in this case (Welzel, 2003; Mück *et al.*, 2003).

The above-described SQUID system was able to detect all relevant defects in niobium sheets with sufficient signal-to-noise ratio. Compared to a conventional system (Elotest with induction coil probe from Rohmann GmbH, Frankenthal, Germany), the measured signal-to-noise ratio was better by a factor of up to 100, see also Fig. 7 (right). The scanning time of about 15 minutes required for a 30×30 cm^2 sheet was limited by the travel speed of the translation stage used; the high sensitivity of the system should allow for a shorter (say, 5 min) scanning time without a noticeable loss in the signal-to-noise ratio.

Eddy-current measurements were performed with a HTS SQUID on aircraft parts (Kreutzbruck *et al.*, 1998) to compare the SQUID NDE system with a commercial eddy-current NDE system (Elotest B1, Rohmann GmbH Frankenthal, Germany) using an induction coil without a ferrite core (PLA-44) as field sensor. The test sample was an aluminum plate with an artificial crack 40 mm long, 0.15 mm wide and 1.2 mm deep, which was covered by another 13 mm-thick aluminum plate. The crack was not detectable with the conventional system when a detection bandwidth of 30 Hz was used. Only in a bandwidth of 2 Hz could the crack be detected; the signal-to-noise ratio was still smaller than 3. With a HTS SQUID system, however, the crack could be detected with a signal-to-noise ratio of about 300 in a much larger bandwidth of 50 Hz.

Tsukamoto *et al.* developed an inspection system using high-T_c SQUID to detect fatigue cracks in steel deck plates covered by asphalt pavement (Tsukamoto *et al.*, 2019). The magnetic signal is picked up by an external pickup coil magnetically coupled to a high-T_c SQUID in magnetic shielding. Eddy currents in the steel plates are induced by a double-D coil. The system is mounted on a hand cart carrying a liquid nitrogen cryostat. Stable operation of the SQUID

system on an expressway bridge in urban area was demonstrated. Electrical discharge machined cracks in steel plates could be detected at stand-off distances of about 100 mm.

H3.4.6 SQUID microscopes

The high spatial as well as the high field sensitivity make SQUID microscopes ideal for nondestructive evaluation of certain types of materials, circuits or devices. For example, local defects, such as scratches and dents, as well as fatigue and mechanical stress can generate a remanent magnetization in certain stainless steels (Seeger *et al.*, 1964). This remanent magnetization can easily be detected with a SQUID (Shaw *et al.*, 1999; Kasai *et al.*, 1997). Reviews of SQUID micrcoscopy can be found in (Fleet *et al.*, 1999; Kirtley, 2015).

At the University of Giessen, the surface of several 1mm-thick stainless steel slabs with artificial scratches and dents was examined with a SQUID microscope (Gruhl *et al.*, 2001). Figure 8 (upper right) shows a photograph of a stainless steel sample with various surface damages: six indentations caused by hammer strikes with various power, and several shallow scratches. The corresponding magnetic field distribution measured with a scanning SQUID microscope is shown in Fig. 8 (lower right). The stainless steel sample was not magnetized prior to the measurement, but was measured unshielded in the earth’s magnetic field. It is found that the remanent magnetization is proportional to the strength of the mechanical stress: one can recognize the correlation between the strength with which the indentations were created and the magnetic field amplitude above the indentations. Although it is possible to measure such samples with conventional sensors by magnetizing the damaged stainless steel slabs, one will then lose the information about the force which with the defects were created. Similar findings were reported elsewhere (Bonavolontà *et al.*, 2007b).

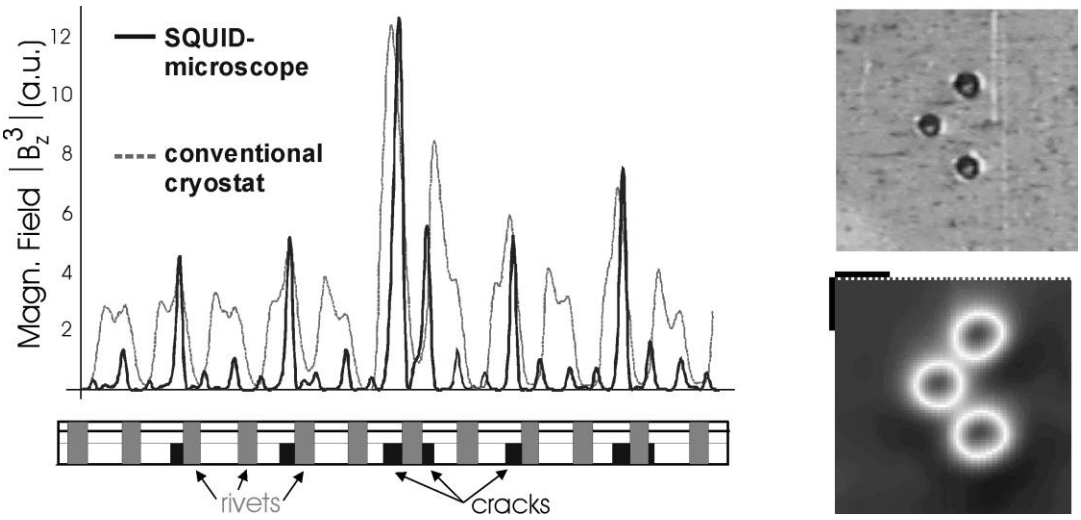

Fig. 8. Nondestructive evaluation using a scanning SQUID microscope. Left: eddy current test of a wing section of an Airbus A-300 showing eddy current field measured with SQUID microscope (solid line) and SQUID in conventional cryostat (dashed line). Cross section of sample consisting of three aluminum layers with rivets (gray vertical bars) and cracks adjacent to rivets (black boxes in lowest aluminum layer) is shown below. Right: optical image (upper) and magnetic image (lower picture) of stainless steel slap with three indentations (scanned area is 5 × 5 mm^2).

SQUID microscopes have also been employed for the nondestructive evaluation of semiconducting circuits and photovoltaic cells. Several methods have been investigated to this end. Microelectronic chips were tested with a HTS SQUID microscope by measuring the magnetic field produced by electric current flowing in the circuits (Fleet *et al.*, 1999). Shorts between pins of a packaged circuit could be identified and located to within ± 35 μm. With a 3D analysis algorithm, the current in stacked integrated circuits of multiple layers of copper planes can be imaged (Gaudestad and Orozco, 2014).

The current density in photovoltaic cells was measured to detect internal shorts in the p-n-junction (Dechert, 1999; Dechert *et al.*, 1999). An open-circuited photovoltaic cell was illuminated and the magnetic field above the cell was recorded. In the absence of internal shorts, no static

magnetic field is produced by the cell. Detecting local fields enabled the authors to precisely locate shorts in the cell junction.

Semiconducting wafers were illuminated with a focused laser beam and the magnetic field of the net photocurrents induced in the sample was measured with a niobium SQUID (Beyer *et al.*, 2001). They were able to detect changes in the doping of semiconducting wafers as well as electrically active defects, such as grain boundaries. They could also localize artefacts in photovoltaic devices. Similar measurements were performed using high T_c SQUIDs (Kong *et al.*, 2007; Nakatani *et al.*, 2011).

Measurements were also performed on aircraft fuselage samples with the LTS SQUID microscope using the eddy current NDE method (Gruhl *et al.*, 2001). Multilayer structures of up to four layers of aluminum sheet of the fuselage of an Airbus A-300 were examined. The samples investigated with the SQUID microscope had a length of about 500 mm and had four rivet rows each containing 21 rivets. Figure 8 (bottom left) shows the cross section of the investigated samples, which consist of three layers of aluminum sheets. The top layer has a thickness of 1.4–2 mm, the second layer one of only 0.6–0.8 mm and the third layer is 1.8–2.5 mm thick. Due to cyclic stress loading, the defects usually occur in the third layer, and the fatigue cracks are most likely to develop along the direction of the fastener row. The titanium rivets had a diameter of 4.8 mm and a distance between each other of 22.5 mm. For eddy current measurements, a single wire positioned perpendicular to the rivet rows was used to excite eddy currents in the sample. The wire was positioned below the SQUID such that the excitation field was minimized at the location of the SQUID. No electronic compensation of the excitation field at the location of the SQUID was used. The excitation frequency was 2 kHz and the separation between sample and SQUID was 600 μm. Figure 8 (left) shows a line scan along a rivet row. In order to distinguish possible defect

signals from signals caused by rivets, the magnetic field data were raised to the third power. Then the amplitudes of the signals generated by cracks are nearly proportional to the crack length. By exciting with a wire the signal of a flawless rivet shows an increase in magnetic field on one side of the rivet and a decrease on the other side. This is caused by induced currents, which flow in clockwise direction on one side and counter-clockwise on the other. A defect induces an additional current, which leads to an increase or decrease of the z-component of the magnetic field, depending on the position of the defect. It can be seen from Fig. 8 that the signals produced by the titanium rivets themselves are small compared to the signals due to cracks. Even a 1.2mm-long crack produces a signal, which is somewhat larger than the signal from a rivet without defect. Also shown in Fig. 8 (left) is a measurement of the same sample, using a SQUID inside a conventional cryostat. The stand-off distance between SQUID and sample here was about 6 mm. As the cracks to be detected are short, and as the distance between the rivets is relatively short as well, the high spatial resolution provided by the SQUID microscope is quite helpful when distinguishing possible defects from the signals generated by the rivets.

H3.4.7 Conclusions

A large number of groups investigated the applicability of SQUIDs for nondestructive evaluation of a great variety of materials, ranging from food to aircrafts. A common find is that especially for the case of thick, highly conductive, or ferromagnetic materials, as well as sintered materials, the SQUID based systems show a much higher sensitivity compared to conventional eddy current, x-ray, or ultrasonic testing. The higher sensitivity, the larger dynamic range and the better low frequency performance of SQUIDs as compared to that of coils, magneto-resistive sensors or flux-gates, does improve the probability of finding a defect, and, more importantly, offers a substantial increase in testing speed. The use of a SQUID is sometimes justified in commercial applications

if the testing speed is increased by a factor of two. These features have led to successful application of SQUID-based electromagnetic inspection to a number of specific NDE problems, including the detection of deep-lying defects in engineering structures such as reactor vessels and bridges, in aircraft structures and components, and for identifying metallic contaminants in industrial products.

Figure Captions

Fig. 1. Basic principle of nondestructive evaluation of ferromagnetic plates using a magnetic field sensor, such as a SQUID (see text).

Fig. 2. Principle of magnetic detection of ruptures in tendon strands of prestressed concrete beams.

Fig. 3. Principle for detection of contaminants in metallic sheets.

Fig. 4. Left: Signal time trace of small metallic ball with different diameter at sheet speed of 9 m/min, and right: Signal time trace of small metallic ball with different diameter at sheet speed of 50 m/min.

Fig. 5. Basic principle of eddy current NDE (left), and measurement configuration used to test niobium sheets with a SQUID (right).

Fig. 6. In-phase SQUID signal track recorded in one rotation of Airbus wheel with artificial inner flaws.

Fig. 7. Left: Two-dimensional distribution of the eddy current field above a 22 cm by 22 cm size niobium sheet. The excitation field generated by a 3-mm diameter coil was about 0.6 mT peak-to-peak; the eddy-current frequency was 10 kHz, measurement time was about 15 minutes. Ta inclusions (bright spots) are clearly detected. Right: Same

sheet measured with conventional eddy-current NDE system. Most defects are obscured by noise. Scanning time and measurement bandwidth same as for SQUID measurement.

Fig. 8. Nondestructive evaluation using a scanning SQUID microscope. Left: eddy current test of a wing section of an Airbus A-300 showing eddy current field measured with SQUID microscope (solid line) and SQUID in conventional cryostat (dashed line). Cross section of sample consisting of three aluminum layers with rivets (gray vertical bars) and cracks adjacent to rivets (black boxes in lowest aluminum layer) is shown below. Right: optical image (upper) and magnetic image (lower picture) of stainless steel slap with three indentations (scanned area is 5×5 mm^2).

References

Bain RJP, Donaldson GB, Evanson S, Hayward G (1985) SQUID gradiometric detection of flaws in ferromagnetic structures. In: SQUID 85 (Hahlbohm HD, Lübbig H, eds), pp 841–846. Berlin: de Gruyter.

Banchet J, Jouglar J, Vuillermoz PL, Waltz P, Weinstock H (1995) Evaluation of stress in steel *via* SQUID magnetometry. In: Review of Progress in QNDE, Vol. 14 (Thompson DO, Chimenti DE, eds), pp. 1675-1682. New York: Plenum Press.

Bellingham JG, Macvicar MLA, Nisenoff M (1987) SQUID technology applied to the study of electrochemical corrosion. IEEE Trans. Mag. 23: 477-479.

Beyer J, Drung D, Schurig T (2001) SQUID photoscanning: an imaging technique for NDE of semiconductor wafers and devices based on photomagnetic detection. IEEE Trans. Appl. Supercond. 11: 1162-1167.

Bick M, Sullivan P, Tilbrook DL, Du J, Gnanarajan S, Leslie KE, Foley CP (2005) A SQUID-based metal detector: comparison to coil and X-ray systems. Supercond. Sci. Technol. 18: 346-351.

Bray, DE, Stanley RK (1989) Nondestructive Evaluation. New York: McGraw-Hill.

Bonavolontà C, Peluso G, Pepe GP, Valentino M (2004) Detection of Early Stage Damage In Carbon Fiber Reinforced Polymers For Aeronautical Applications Using An HTS SQUID Magnetometer. Eur. Phys. J. B 42: 491-496.

Bonavolontà C, Valentino M, Pepe GP (2007) Characterization of the damage process in GLARE 2 using an eddy current technique based on HTS-SQUID magnetometer. Supercond. Sci. Technol. 20: 51-56.

Bonavolontà C, Valentino M, Adamo M, Sarnelli E (2007a) Detection of plastic deformation in structural steel using scanning SQUID microscopy. Meas. Sci. Technol. 18: 2116-2120.

Bonavolontà C, Valentino M, Peluso G, Penta F, Di Iorio A (2009) Detection of mechanical fatigue in structural steel using SQUID and flux-gate sensors. Journal of Superconductivity and Novel Magnetism 22: 833-839.

Braginski AI (2011) Application to nondestructive evaluation of materials and structures. In: 100 years of superconductivity (Rogalla H, Kes PH, eds), p. 342-349. Boca Raton: CRC Press.

Capobianco TE, Moulder JC, Fickett FR (1986) Flaw detection with a magnetic field gradiometer. In: Proc. 15th Symposium on NDE, (Moore DW and Matzkanin GA, eds), p. 15, San Antonio: NDE Testing Information Analysis Center.

Clarke J, Braginski AI (eds) (2006) The SQUID handbook, Vol. II. Weinheim: Wiley-VCH.

Dechert J (1999) Hochauflösende Raster-SQUID Mikroskopie. PhD Thesis, University of Giessen.

Dechert J, Mück M, Heiden C (1999) A scanning SQUID microscope for samples at room temperature. IEEE Trans. Appl. Supercond. 9: 4111-4114.

Donaldson GB, Evanson S, Otaka M, Hasegawa K, Shimizu T, Takaku K (1990) Use of a SQUID magnetic sensor to detect ageing effects in duplex stainless steels. Bri. J. NDT. 32: 238–240.

Donaldson GB, Cochran A, McKirdy DMcA (1996) The use of SQUIDs for nondestructive evaluation. In: SQUID Sensors: Fundamentals, Fabrication and Applications (Weinstock H, ed), pp 599–628. Dordrecht: Kluwer.

Evanson S, Bain RJP, Donaldson GB, Stirling DG, Hayward G (1993) A comparison of the performance of planar and conventional second-order gradiometers coupled to a SQUID for the NDT of steel plates. IEEE Trans. Magn. 25: 1200-1203.

Faley MI *et al.* (1999) Operation of the HTS dc-SQUID Sensors in High Magnetic Fields. IEEE Trans. Appl. Supercond. 9: 3386-3391.

Fleet EF, Chatraphorn S, Wellstood FC, Knauss LA (1999) HTS scanning SQUID microscopy of active circuits. IEEE Trans. Appl. Supercond. 9: 4103-4106.

Gaudestad J, Orozco A (2014) Magnetic Field Imaging for non destructive 3D IC testing. Microelectronics Reliability 54:2093-2098.

Ghorbanpoor A (1998) Magnetic-based NDE of steel in prestressed and post-tensioned concrete bridges. In Proc. Structural Materials Technology III, Vol. 3400 (Medlock RD, Laffrey DC, eds), pp. 343-347. San Antonio: SPIE.

Graham D, Maas P, Donaldson GB, Carr C (2004) Impact damage detection in carbon fibre composites using HTS SQUIDs and neural networks. NDT & E International 37: 565–570.

Gruhl F, Mück M, Kreutzbruck Mv, Dechert J (2001) A scanning superconducting quantum interference device microscope with high spatial resolution for room temperature samples. Rev. Sci. Instrum. 72**:** 2090-2096.

Hatsukade Y *et al.* (2013) SQUID NDE on braided carbon fiber reinforced polymers with middle-end fibers under step-by-step tensile loading. IEEE Trans. Appl. Supercond 23: 1603205.

Hatsukade Y, Masutani N, Teranishi S, Masamoto K, Kanenaga S, Adachi S, Tanabe K (2017) HTS-SQUID NDE technique for pipes based on ultrasonic guided wave. J. Phys. Conf. Ser. 871: 012072.

Hibbs AD, Chung R, Pence JS (1993) Corrosion current measurement with a high resolution scanning magnetometer. In: Review of progress in quantitative NDE, Vol. 13A, (Thomson DO, Chimenti DE, eds), pp. 1955-1962. New York: Plenum Press.

Hohmann R *et al.* (1999) Aircraft wheel testing with machine-cooled HTS SQUID gradiometer system. IEEE Trans. Appl. Supercond. 9: 3801–3804.

Hohmann R, Lomparski D, Krause HJ, Kreutzbruck Mv, Becker W (2001) Aircraft wheel testing with remote eddy current using a HTS SQUID magnetometer. IEEE Trans. Appl. Supercond. 11: 1279-1282.

Horng HE, Jeng JT, Yang HC, Chen JC (2002) Evaluation of the flaw depth using high-Tc SQUID. Physica C 367: 303-307.

Kasai N, Ishikawa N, Yamakawa H, Chinone K, Nakayama S, Odawara A (1997) Nondestructive detection of dislocations in steel using a SQUID gradiometer. IEEE Trans. Appl. Supercond. 7: 2315-2318.

Keenan ST, Romans EJ (2012) Compensated high temperature SQUID gradiometer for mobile NDE in magnetically noisy environments. NDT & E International 47:1-6.

Keiji T, Yasuaki M, Yuta N, Ryota I, Kayo F, Kenji S, Toshihiko K (2017) Magnetic method for measuring moisture content using diamagnetic characteristics of water. Meas. Sci. Technol. 28: 014010.

Kirtley J (2015) Scanning SQUID microscopy. In: Applied Superconductivity. Handbook on Devices and Applications, Vol. 2 (Seidel P, ed), pp. 1042-1065. Weinheim: Wiley-VCH.

Kong XY, Kojima K, Sakuta K, Itozaki H (2007) Current vector distribution in semiconductor observed by laser SQUID microscope with needle. Physica C 463-465: 1048-1051.

Krause HJ *et al.* (1997) Mobile HTS SQUID System for Eddy Current Testing of Aircraft, In: Review of Progress in QNDE, Vol. 16 (Thompson DO, Chimenti DE, eds), pp. 1053-1060. New York: Plenum Press.

Krause HJ *et al.* (2002) SQUID array for magnetic inspection of prestressed concrete bridges. Physica C 368: 91-95.

Krause HJ *et al.* (2005) Detection of Magnetic Contaminations in Industrial Products Using HTS SQUIDs. IEEE Trans. Appl. Supercond. 15: 729-732.

Krause HJ, Donaldson G (2006) Nondestructive evaluation of materials and structures using SQUIDs. In: The SQUID handbook, Vol. II. (Clarke J and Braginski AI, eds), pp. 441-479. Weinheim: Wiley-VCH.

Krause HJ, Mück M, Tanaka S (2015) SQUIDs in nondestructive evaluation. In: Applied Superconductivity. Handbook on Devices and Applications, Vol. 2 (Seidel P, ed), pp. 977-991. Weinheim: Wiley-VCH.

Kreutzbruck Mv, Baby U, Mück M, Heiden C (1998) Experiments on eddy current NDE with HTS rf SQUIDs. In: Studies in Applied Electromagnetics and Mechanics, Vol. 13, pp. 165–168, Amsterdam: IOS Press.

Kreutzbruck Mv, Baby U, Theiss A, Mück M, Heiden C (1999) Inspection of aircraft parts with high remanent magnetization by eddy current SQUID NDE. IEEE Trans. Appl. Supercond. 9: 3805-3808.

Kreutzbruck Mv (2004) Unrivalled sensitivity – SQUIDs in NDT. In: High Temperature Superconductivity, Vol. 2 (Narlikar AV, ed), pp. 223-297. Berlin: Springer.

Lima EA, Irimia A, Wikswo JP (2006) The magnetic inverse problem. In: The SQUID handbook, Vol. II (Clarke J and Braginski AI, eds), pp. 139-267. Weinheim: Wiley-VCH.

Ma YP, Wikswo JP (1995) Techniques for depth-selective, low-frequency eddy current analysis for SQUID-based nondestructive testing. J. NDE 14: 149-167.

Miyazaki Y, Arai Y, Nagashima K, Itozaki H (2012) Detection of White Layer on Rail by Using SQUID. In: Applied Electromagnetic Engineering for Magnetic, Superconducting and Nano Materials (Mamalis AG, Kladas A, Enokizono M, eds), pp 225-230.

Mück M, Welzel C, Farr A, Schölz F, Singer W (2003) Nondestructive testing of niobium sheets for superconducting resonators. IEEE Trans. Appl. Supercond. 13: 239-244.

Nagaishi T, Ota H, Nishi K, Kuwa K, Fujita T, Tanaka S (2007) First Practical High Tc SQUID System for the Detection of Magnetic Foreign Substances in Commercial Products. IEEE Trans. Appl. Supercond. 17: 800-803.

Nakatani Y, Hayashi T, Itozaki H (2011) Observation of Polycrystalline Solar Cell Using a Laser-SQUID Microscope. IEEE Trans. Appl. Supercond. 21: 416-419.

Ruosi A, Pepe G, Peluso G, Valentino M, Monebhurrun V (1999) Experimental and numerical results of electromagnetic nondestructive testing with HTc SQUIDs. IEEE Trans. Appl. Supercond. 9: 3499-3502.

Ruosi A, Valentino M, Lopresto V, Caprino G (2002) Magnetic response of damaged carbon fibre reinforced plastics measured by a HTS-SQUID magnetometer. Composite Structures 56: 141–149.

Sawade G, Krause HJ, Gampe U (1997) Non Destructive Examination of Prestressed Tendons by the Magnetic Stray Field Method. In Proceedings of the 7th international conference on Structural Faults and Repair – 97, Vol. I (Forde MT, ed), pp. 401-406. Edinburgh: Engineering Technical Press.

Sawade G, Krause HJ (2010) Magnetic and electromagnetic non-destructive techniques for post-tensioning. In: COST 534, New Materials, Systems, Methods and Concepts for Prestressed Concrete Structures (Polder RB *et al.*, eds) pp. 209-240. Delft: COST Office.

Sawade G, Krause HJ (2010a) Prüfung von Spannbetonbauteilen mit magnetischen Methoden. Beton- und Stahlbetonbau 105: 154-164.

Shaw TJ, Schlenga K, McDermott R, Clarke J, Chan JW, Kang SH, Morris JW (1999) High-T_c SQUID microscope study of the effects of microstructure and deformation on the remanent magnetization of steel. IEEE Trans. Appl. Supercond. 9: 4107-4110.

Tanaka S *et al.* (2006) A food contaminant detection system based on high-Tc SQUIDs. Supercond. Sci. Technol. 19: S280-S283.

Tanaka S, Fujita H, Hatsukade Y, Otani T, Suzuki S, Nagaishi T (2007) A High Tc SQUID Micro-detector with a high performance magnetic shield for industrial products. Supercond. Sci. Technol. 20: S385-S388.

Tanaka S, Akai T, Hatsukade Y, Otani T, Ikeda Y, Suzuki S, Tanabe K (2009) High Tc SQUID Detection System for Metallic Contaminant in Lithium Ion Battery. IEEE Trans. Magn. 45: 4510-4513.

Tanaka S, Akai T, Kitamura Y, Hatsukade Y, Otani T, Suzuki S (2011) Two-Channel HTS SQUID Gradiometer System for Detection of Metallic Contaminants in Lithium-Ion Battery. IEEE Trans. Appl. Supercond. 21: 424-427.

Tavrin Y, Krause HJ, Wolf W, Glyantsev V, Schubert J, Zander W, Bousack H (1996) Eddy current technique with high temperature SQUID for non-destructive evaluation of non-magnetic metallic structures. Cryogenics 36: 83–86.

Tavrin Y, Siegel J, Hinken J (1999) Standard method for detection of magnetic defects in aircraft engine discs using a HTS SQUID gradiometer. IEEE Trans. Appl. Supercond. 9: 3809–3812.

Thomas IM, Ma YP, Wikswo JP (1993) Spatial resolution and sensitivity of magnetic susceptibility imaging. IEEE Trans. Appl. Supercond. 3: 1937-1940.

Tsukamoto A, Hato T, Adachi S, Oshikubo Y, Tsukada K, Tanabe K (2019) Development of three-channel HTS-SQUID inspection system for orthotropic steel decks of expressway bridges. IEEE Trans. Appl. Supercond. 29: 1601505

Weinstock H, Erber T, Nisenoff M (1985) Threshold of Barkhausen emission and onset of hysteresis in iron. Phys. Rev. B31: 1535-1553.

Weinstock H, Nisenoff M (1985) Nondestuctive evaluation of metallic structures using a SQUID gradiometer. In: SQUID’85 (Hahlbohm HD, Lübbig H, eds), pp. 853-860. Berlin: de Gruyter.

Weinstock H, Tralshwala N, Claycomb JR (1999) Nondestructive evaluation of wires using high-temperature SQUIDs. IEEE Trans. Appl. Supercond. 9: 3797-3800.

Welzel C (2003) PhD Thesis, University of Giessen.

Wikswo JP, Ma YP, Sepulveda NG, Tan S, Thomas I, Lauder A (1993) Magnetic susceptibility imaging for nondestructive evaluation. IEEE Trans. Appl. Supercond. 3: 1995-2002.

Wikswo JP (1995) SQUID magnetometers for biomagnetism and nondestructive testing: important questions and initial answers. IEEE Trans. Appl. Supercond. 5: 74–120.

Wikswo JP (1996) The magnetic inverse problem for NDE. In: SQUID Sensors: Fundamentals, Fabrication and Applications (Weinstock H, ed), pp 629–695. Dordrecht: Kluwer.

Wunderlich S, Schmidl F, Specht H, Dörrer L, Schneidewind H, Hübner U, Seidel P (1998) Planar gradiometers with high- DC SQUIDs for non-destructive testing. Supercond. Sci. Technol. 11: 315-321.

Yoshida K, Kage T, Suzuki T, Hatsukade Y, Tanaka S (2014) Development of Robust HTS-SQUID for Non-destructive Inspection System in Unshielded Environment. J Phys: Conf Ser 507: 042049.